

NEOTECTONIC EVOLUTION OF NORTHEASTERN VENEZUELA. PALEOMAGNETIC EVIDENCE OF BLOCK ROTATION OF THE SERRANÍA DEL INTERIOR RANGE

EVOLUCIÓN NEOTECTÓNICA DEL NORESTE DE VENEZUELA. EVIDENCIA PALEOMAGNÉTICA DE ROTACIÓN DE BLOQUES DE LA SERRANÍA DEL INTERIOR

Atiria Fajardo^{a}, Charles Aubourg^b, Bertrand Niviere^b, Redescal Uzcátegui^c, François Demory^d*

ABSTRACT

In Northeastern Venezuela, the last 10 Ma wrenching component between the Caribbean and South American plates is accommodated by E-W strike-slip movement along the El Pilar fault, causing shortening in the eastern Serranía del Interior (SDI). However, evidence of active compression has been identified in the southern limit of the SDI, in the Monagas Fold and Thrust Belt (MFTB). The objective of this study is to show that the active tectonics in northeast Venezuela is related to block rotation in the SDI caused by the wrenching component of the El Pilar fault.

An exploratory paleomagnetic survey was conducted in the Caripe and Bergantín blocks of the SDI. A key finding was a magnetization component of normal and reverse polarities with a southwest deviation and a negative bedding-tilt test, indicating that this component was acquired when the folding process in the SDI stopped. The average declination indicates a clockwise block rotation of $37^\circ \pm 4^\circ$ and a post-middle Miocene rotation rate of $3.7^\circ/\text{Ma}$ in both blocks. This regional clockwise rotation is related to the development of a synthetic Riedel shear system formed by the El Pilar fault as the master regional fault and by the Urica and San Francisco faults as synthetic Riedel shears.

RESUMEN

En el noreste de Venezuela, durante los últimos 10 Ma el movimiento desstral entre las placas del Caribe y América del Sur es acomodado por un movimiento de rumbo E-W a lo largo de la falla de El Pilar que también causa un acortamiento en la Serranía del Interior oriental (SDI). Sin embargo, se han identificado evidencias de compresión activa en el límite sur de la SDI, en el cinturón de pliegues y corrimientos de Monagas (MFTB). El objetivo de este estudio es mostrar que la tectónica activa en el noreste de la cuenca Oriental está relacionada con la rotación de bloques en la SDI provocada por la componente rumbo-deslizante de la falla de El Pilar.

Se realizó un levantamiento paleomagnético exploratorio en los bloques Caripe y Bergantín del SDI. Un hallazgo clave fue una componente de magnetización de polaridades normales e inversas con una desviación suroeste y un test de rotación de capa negativo, lo que indica que esta componente se adquirió posteriormente al plegamiento de la SDI. La declinación promedio indica una rotación de bloques en el sentido horario de $37^\circ \pm 4^\circ$ y una tasa de rotación post Mioceno Medio de $3.7^\circ/\text{Ma}$, en ambos bloques. Esta rotación regional horaria está relacionada con el desarrollo de un sistema sintético de cizalla Riedel formado por la falla de El Pilar como falla regional maestra y por las fallas Urica y San Francisco como cizallas sintéticas Riedel.

Keywords: Caribbean, Riedel system, Pilar fault, Urica fault Caripe block, Bergantín block.

Palabras clave: Caribe, sistema Riedel, Falla de El Pilar, Falla de Urica, Bloque Caripe, Bloque Bergantín.

1. Introduction

Since the Oligocene, oblique collision between the Caribbean and South American plates has been forming the Serranía del Interior (SDI), the Monagas Fold and Thrust Belt (MFTB)

and the Maturín Foreland sub-basin (Figure 1). Many authors developed geological interpretations, structural models, tectono-sedimentary analyses, and stratigraphic models from the Cretaceous to middle Miocene, in order to understand

a. Geohidra Consultores, C.A., Caracas, Venezuela. fajardoaq@gmail.com.

b. Université de Pau et des Pays de l'Adour, E2S UPPA, CNRS, TOTAL, LFCR, Pau, France. charles.aubourg@univ-pau.fr, bertrand.niviere@univ-pau.fr.

c. Universidad Simón Bolívar, Caracas, Venezuela. rutzcategui@usb.ve.

d. CEREGE, Aix en Provence, France. demory@cerege.fr.

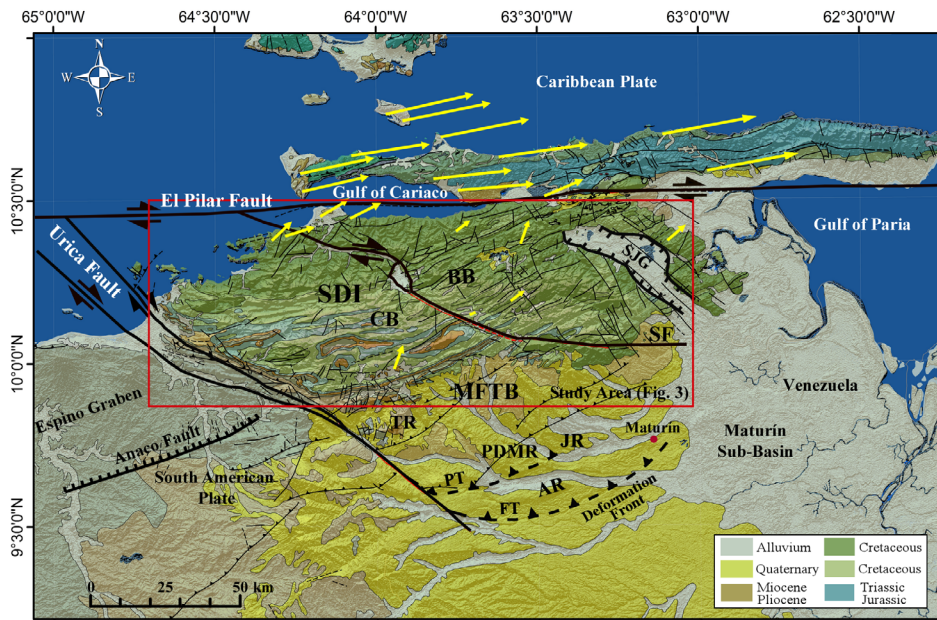


Figure 1. Tectonic map of the Northeastern Venezuela. SDI: Serranía del Interior; MFTB: Monagas Fold and Thrust Belt; SFF: San Francisco Fault; CB: Caripe Block; BB: Bergantin Block; UF: Urica Fault; TR: Tarragona Ridge; TT: Tarragona Thrust; PT: Pirital Thrust; PH: Pirital High; FT: Furrial Thrust; AR: Amarilis Ridge; ABT: Amarilis Back Thrust; JT: Jusepín Thrust; SJG: San Juan Graben. Velocity model with structural interpretation modified from [9].

the regional tectonics [1, 2, 3, 4, 5]. In addition, many studies have been motivated by hydrocarbon exploration within the Maturín sub-basin, specifically in the MFTB, showing folding of the post-Miocene sequences and suggesting deformation younger than 10-12 Ma [6, 7, 8].

Moreover, several near surface studies have identified active faults, recent deformation and river terraces in the SDI southern limit and in the MFTB (e.g. [10, 11, 12, 13, 14] where active tectonics have been studied through geodetic, seismic data, focal mechanisms analysis and GPS studies [15, 16, 17]). In strike-slip faults systems, block rotation may often be observed along vertical axis; and because of this, we performed an exploratory paleomagnetic survey in the SDI for first time, in order to collect additional regional kinematical data to better understand the neotectonic activity in the Northeastern Venezuela. Finally, we have integrated the paleomagnetic data in the SDI with the geomorphological and seismic data obtained in the MFTB by [18] to propose a Neogene kinematic model controlled by the El Pilar, Urica and San Francisco strike-slip faults.

2. Geological setting

The Northeastern Venezuela Basin is located between the latitudes 8°N and 11°N and the longitudes 61°W and 66°W and this was shaped by four major tectonic phases [19, 20, among many others], a Paleozoic Pre-rift phase, followed by a Jurassic rifting phase, then a Cretaceous - Early Oligocene passive margin phase and finally a late Oligocene - Holocene

active margin phase (Figure 2). At the beginning of the active margin phase, the northern boundary of South America was affected by the diachronous migration of the Caribbean plate eastward, defined as a transpressive movement [21, 22, 23, 24]. This transpressive movement is interpreted as a strain partitioning system which is accommodated by a northern region of strike-slip deformation and a southern region of fold-thrust belt contraction. This fold-thrust belt system can be seen in the eastern Venezuela (Figure 1): The SDI (hinterland), the Pirital belt and the Furrial belt (foothill), these last two located in the MFTB [24].

During the last 10 Ma the advance of the Caribbean foredeep has been ~20 mm/y eastward, with a change

in the azimuth movement from N85° to N70° of the northern part of the Caribbean plate with respect to the North American plate and from N100° to N85° of the southeastern part of the Caribbean plate with respect to the South American plate [25, 26, 27, 28, 29]. This change from east-southeast transpression to eastward translation controls the neotectonic activity in the SDI and the MFTB [30, 31].

In the SDI mountains are exposed rocks of the Cretaceous - early Oligocene passive margin inverted from the middle Eocene to the Miocene, and affected by thick-skin tectonic with shortening ranging from 16 km to 120 km. Apatite fission track data show that the shortening in the eastern SDI ceased at ~12 Ma [32]. The SDI is limited by the El Pilar fault to the north. This fault is a 350 km long right-lateral strike-slip fault active since the late Miocene [33, 12] and in Venezuela concentrates the present's day E-W Caribbean plate movement relative to South America [16].

To the south, The SDI is limited by the Pirital thrust system fault and across by the right-lateral Urica and San Francisco faults to the west and east, respectively (Figure 1). The Urica fault is a NW-SE ~107 km-long right-lateral strike-slip fault active since the Miocene, probably an inherited feature from an pre-existing rift of Cambrian age [34, 7]. Audemard *et al.* [35] proposed that this fault is one of the synthetic Riedel shear related to the interaction between the Caribbean and South America plates. The Urica fault southern trace merges with the frontal thrusts between the MFTB and the deformation front [36, 7, 18]; however, the western trace is not well defined but

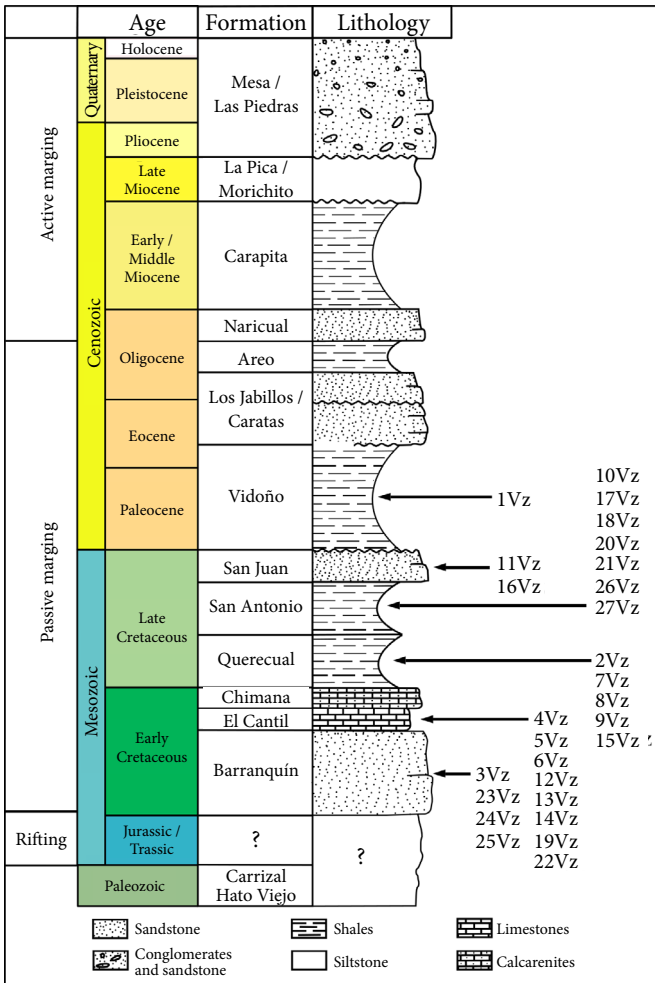


Figure 2. Stratigraphic chart of the Northeastern Venezuela Basin with geological formations sampled in the SDI.

it may continue westward as a southerly dipping normal fault [36, 7]. The San Francisco right-lateral fault divides the SDI into two blocks, the Bergantín Block to the west and Caripe Block to the east [37]. This fault is NW-SE oriented and exhibits 18 - 40 km of offset within the SDI [38] and it starts in the Gulf of Cariaco to the north and then follows to eastward where is oriented E-W until disappearing beneath the Plio-Quaternary series in the northern area of the city of Maturín [39, 7] (Figure 1).

3. Method

3.1 Fieldwork

Data analysis was performed using PaleoMac software [40]. Principal Components Analysis was used to obtain best-fit lines and calculate paleomagnetic components [41],

and Fisher statistics used to calculate mean directions and estimate its uncertainty, the 95% level of confidence and the scattering parameter k [42]. Due to the dense vegetation and the scarcity of paved roads in the study area, we couldn't find outcrops located at both limbs of anticline or syncline structures in order to perform the fold progressive un-tilting test. Therefore, we carried-out a bed-tilting test: is this test each *in situ* paleomagnetic component is rotated along the local bed strike direction by the amount of the dip of the beds until bedding is horizontal, if directions are better grouped after adjusting then the magnetization was acquired before tilting, but if dispersion increases after adjusting for tilt, then the magnetization is post-folding [41].

In order to performance paleomagnetic survey, samples were taken from a total of 27 sites distributed in the SDI mountains (Bergantín and Caripe blocks) to the east of the Urica fault and to east and west of the San Francisco fault (Figure 3). Using a portable gasoline driller, 159 oriented cores of 25 mm diameter were collected and, in addition, 42 oriented blocks which were drilled in the laboratory. The sampled section include rocks from the Cretaceous to the middle Oligocene (Figure 2), compose mainly of: 1) limestone, black shale and calcareous sandstone from the Querecual Formation (2Vz, 7Vz, 8Vz, 9Vz, 10Vz, 15Vz, 17Vz, 18Vz, 20Vz, 21Vz, 22Vz, 26Vz and 27Vz sites) and from the San Juan and San Antonio Formations (16Vz, 7Vz, 8Vz, 9Vz, 10Vz, 11Vz, 15Vz, 16Vz, 17Vz, 18Vz, 20Vz, 21Vz, 22Vz, 26Vz, and 27Vz sites); 2) limestone from the Cantil Formation (4Vz, 5Vz, 6Vz, 12Vz, 13Vz, 14Vz, 17Vz and 19Vz sites); 3) calcareous sandstone, limestone and black shale from El Cantil and Barranquín Formations (3Vz, 23Vz, 24Vz and 25Vz sites); and 4) black shale from the Vidoño Formation (1Vz site). Fifteen oriented samples were taken from each one of the 11 sites drilled and 3 or 4 oriented blocks from the others 16 sampled sites (Table 1).

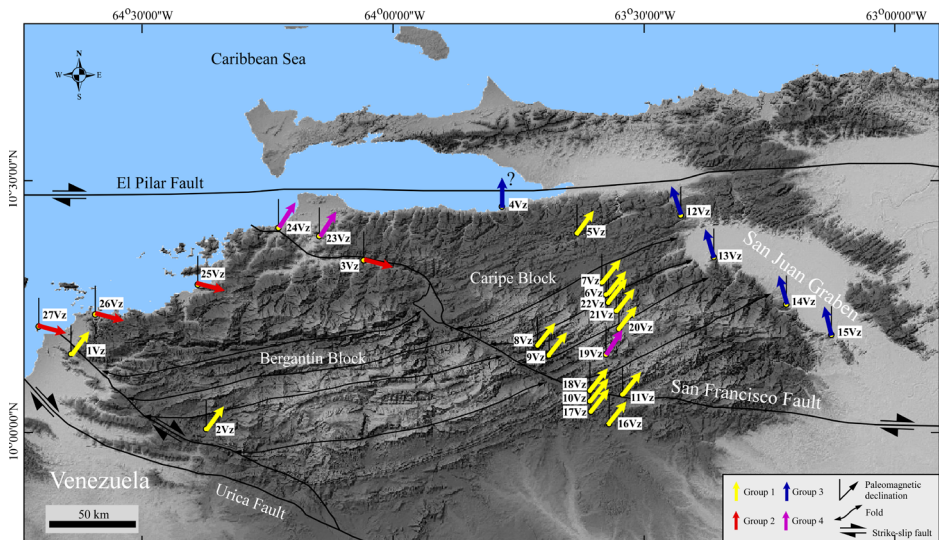


Figure 3. DEM image of the SDI with sampled sites. Arrows indicate paleomagnetic declination for each site. See Figure 1 for location. Base imagen modified from [43].

Table 1. Paleomagnetic data

Site	Latitude	Longitude	Formation	Specimens analyzed by site
5Vz	10°23'29"	63°37'58"	El Cantíl Formation	5
19Vz	10°09'02"	63°34'18"	El Cantíl Formation	5
4Vz	10°26'46"	63°46'55"	Barranquín Formation	7
3Vz	10°20'15"	64°03'31"	Barranquín Formation	8
11Vz	10°04'8"	63°32'22"	San Juan Formation	2
16Vz	10°00'39"	63°34'00"	San Juan Formation	3
10Vz	10°04'58"	63°41'23"	San Antonio Formation	2
17Vz	10°02'23"	63°36'5"	San Antonio Formation	2
18Vz	10°05'34"	63°36'18"	San Antonio Formation	2
1Vz	10°09'01"	64°38'49"	Vidoño Formation	4
2Vz	09°59'59"	64°22'26"	Querecual Formation	5
23Vz	10°23'17"	64°08'51"	Barranquín Formation	4
24Vz	10°24'17"	64°13'44"	Barranquín Formation	3
26Vz	10°13'51"	64°35'51"	San Antonio Formation	6
27Vz	10°12'25"	64°42'37"	San Antonio Formation	2
25Vz	10°17'25"	64°23'27"	Barranquín Formation	2
21Vz	10°14'16"	63°33'11"	San Antonio Formation	4
20Vz	10°12'05"	63°32'44"	San Antonio Formation	4
6Vz	10°16'14"	63°35'19"	El Cantíl Formation	5
22Vz	10°15'20"	63°35'08"	El Cantíl Formation	2
8Vz	10°09'55"	63°42'38"	Querecual Formation	6
9Vz	10°09'47"	63°36'23"	Querecual Formation	5
12Vz	10°25'49"	63°25'20"	El Cantíl Formation	4
13Vz	10°20'38"	63°21'28"	El Cantíl Formation	3
14Vz	10°14'57"	63°12'39"	El Cantíl Formation	4
7Vz	10°17'34"	63°34'47"	Querecual Formation	5
15Vz	10°11'22"	63°07'15"	Querecual Formation	3

3.2 Sample preparation and paleomagnetic measurements

Preparation of samples for paleomagnetic analysis was performed in the laboratories of the University of Pau (France) and the University of Burgos (Spain). The thermal and alternating-field demagnetization processes were performed at the University of Provence (CEREGE, France) and at the University of Burgos and Centro Nacional de Investigación de la Evolución Humana (CENIEH, Spain). The following equipment was used, at the University of Provence: Automated AF demagnetizing SQUID 2G. At the University of Burgos: a) Superconductor magnetometer 2G-755 with automatic sample holder, alternating fields system and ARM inducer, all automatic and synchronized, b) Helmholtz coil system (6 m^3) self-compensated (in-house design and manufacturing) with automatic power triaxial fluxgate MR-3, and c) Thermal demagnetizer TD48-DC (ASC). The processing of the data obtained from the sample demagnetization in the laboratory was carried out with Remasoft 3.0 software.

The 25 mm diameter core samples were cut in specimens of 2.2 cm long, obtaining one to five 10 cc standard specimens. Thermal demagnetization and Alternative Magnetic Field demagnetization (AF) have been used. The protocol followed for the thermal demagnetization specimens consisted of heating every 30°C from 50°C up to 450°C (12 heating steps). For the AF method, high alternating magnetic fields were progressively applied (5 mT up to 100 mT). In order to achieve uniform demagnetization during the demagnetization process, each specimen was placed in a sample holder capable of rotating in three directions of space (x, y, z planes).

Data treatment was performed using PaleoMac software [40]. Principal component analysis was used to extract component. Fisher statistics was used to calculate the mean component. The confidence at 95% is provided (α_{95}) as well as the scattering parameter (k). As commonly used in paleomagnetic study, a tilt test was performed. It consists in restoring bedding to the horizontal using its strike, and this correction is applied to the paleomagnetic component. In this study, as the ChRM is post-folding, incremental fold test was not used, since it is dealing essentially with the *in situ* declination.

4. Results

Paleomagnetic components were compared to the expected apparent polar wander path (APWP) for the last 10 Ma ($\text{APWP}_{0-10\text{Ma}}$; $D = 2^\circ$, $I = 11^\circ$) [44]. Note that the inclination of both Geocentric Axial Dipole (GAD) and the Earth Magnetic field (EMF) at this locality are more inclined than the APWP ($I_{\text{GAD}} = 20^\circ$; $I_{\text{EMF}} = 35^\circ$). Besides, the calculation of block rotation can be inferred directly from the value of declination.

4.1 General pattern

Paleomagnetic components could be extracted in 92% of the samples (Table 2). The pattern of demagnetization reveals the presence of a viscous remanent magnetization (VRM) of normal polarity in 23% of the specimens (Figure 4A). It groups fairly well close to GAD or EMF in geographic coordinates ($D = 359^\circ$, $I = 35^\circ$, $k = 42$, $\alpha_{95} = 4^\circ$) but scatters largely after tilting back the bedding to the horizontal ($D = 1^\circ$, $I = 63^\circ$, $k = 4$, $\alpha_{95} = 15^\circ$) (Figure 5). This component was generally removed at low

Table 2. Paleomagnetic data

Zone	Site	Bedding	Specimens analyzed by site	Geo by site		Geo by zone				Tecto (Tilt Corr) by zone											
				D	I	D	I	K	α_{95}	D	I	K	α_{95}								
East of the Urica fault	1Vz	210/90	4	24	25	29	34	22	10	162	61	19	11								
	2Vz	204/80	5	30	30		--	95	46	7	19	127	49								
	25Vz	14/48	2	--	--		--			127	49	5	24								
	26Vz	238/35	6	97	38		--			49	5	24									
	27Vz	258/32	2	97	38																
Northeast of the San Francisco fault	3Vz	170/73	8	290	-24	294	-91	16	14	287	34	16	14								
	23Vz	160/85	4	114	73	39	68	10	20	347	27	3	42								
	24Vz	320/34	3	114	73																
South of the San Francisco fault	8Vz	355/35	6	45	31	37	29	18	11	26	7	17	11								
	9Vz	344/35	5	45	31																
	10Vz	297/32	2	31	28																
	11Vz	297/32	2	31	28	32	39	21	10	10	42	21	10								
	16Vz	320/10	3	105	30																
	17Vz	010/60	2	105	30																
	18Vz	295/30	2	105	30																
Center of the Caripe block	6Vz	152/44	5	300	-64	25	37	25	8	60	51	13	11								
	20Vz	197/29	4	300	-64																
	21Vz	186/82	4	300	-64																
	22Vz	25/44	2	300	-64																
East of the Caripe block	12Vz	190/32	4	156	32	165	37	25	8	164	-20	9	16								
	13Vz	002/75	3	169	30																
	14Vz	--	4	Possible fallen block																	
	15Vz	008/63	3	169	30																
(Interpreted individually)	4Vz	206/26	7	355	26	355	26	16	15	346	57	12	22								
	5Vz	329/85	5	34	31	34	21	24	16	24	-19	24	16								
	19Vz	195/81	5	36	66	36	66	21	17	348	27	7	31								
(Not interpreted)	7Vz	--	5	--	--	--	--	--	--	--	--	--	--								

temperature (100-350°C) and is weakly coercive (25-35 mT). The VRM has an inclination of ~35° steeper than the APWP or GAD, but consistent with the present day's inclination of Earth magnetic field (Figure 5).

Apart VRM, 63% of the specimens yields one stable component until the complete demagnetization process. Linear segments of these ChRM are converging toward the origin (Figure 4B and 4C). We refer this behavior as Characteristic Remanent Magnetization (ChRM). Other specimens (14%) display paleomagnetic components, but different from the VRM and ChRM (Figure 4D). Some ChRM like components had unblocking temperature up to 450°C and coercivity range up to 100 mT. Only 15Vz and 17Vz sites do not display reliable components. All ChRM components were plotted together *in situ* and after bedding correction was made (Figure 6). Normal (85%) and reverse (15%) polarities equally represented. *In situ*, the component is reasonably well-grouped and easterly deviated

(D = 36°, I = 31°, k = 10, $\alpha_{95} = 4^\circ$). This inclination is consistent with the GAD or EMF inclination. After restoring the bedding to the horizontal, components are much more scattered (D = 46°, I = 41°, k = 4, $\alpha_{95} = 11^\circ$). ChRM are therefore essentially post-tilted, and evidence of remagnetization process.

4.2 Regional analysis of ChRM components

To perform the statistical analysis and estimate block rotation in the SDI we divided the study area in 5 zones. In each zone we grouped sites depending on its paleomagnetics parameters (inclination and declination), geographic location, and the local structural setting.

4.2.1 East of the Urica fault (Bergantín block)

This zone is defined by 1Vz, 2Vz, 25Vz, 26Vz and 27Vz sites and it is located in the Bergantín block of the SDI (Figure 3). The first analysis was carried out for the 1Vz and 2Vz sites located

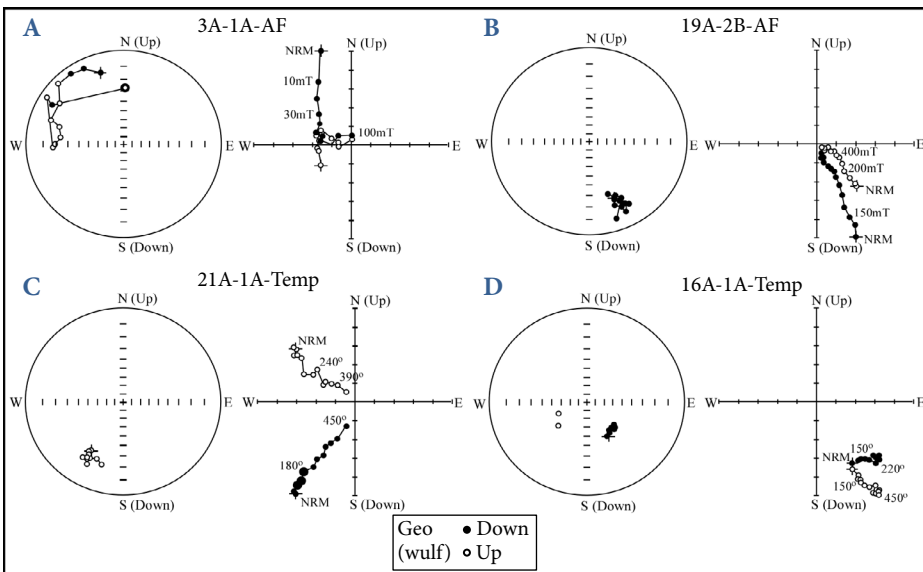


Figure 4. Zijderveld diagrams and stereographic Wulff projections examples of magnetization directions obtained from the sites sampled in the SDI.

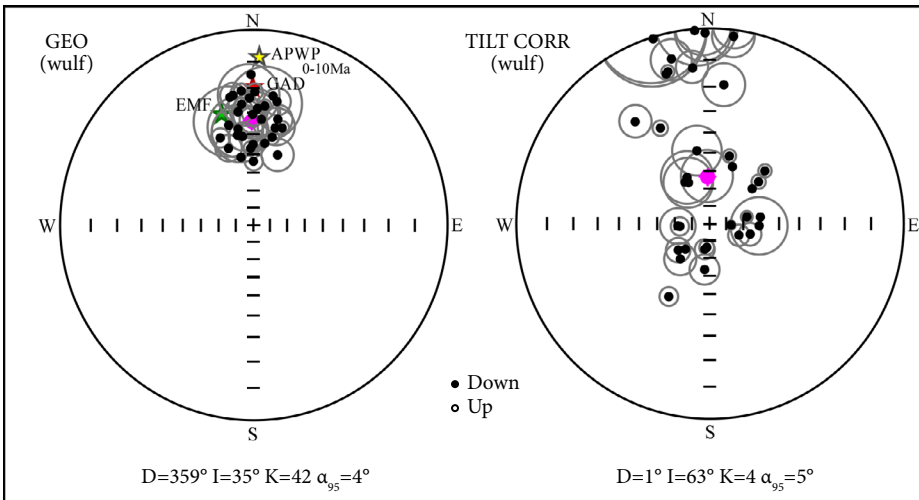


Figure 5. Component VRM. Stereographic projection *in situ* (Geo) and after bedding correction (Tilt Corr). The yellow star represents the expected direction from APWP_{0-10 Ma} in the area. The green star represents the EMF (present day dipole) in the area. The red point represents the present Geocentric Axial Dipole (GAD) in the area.

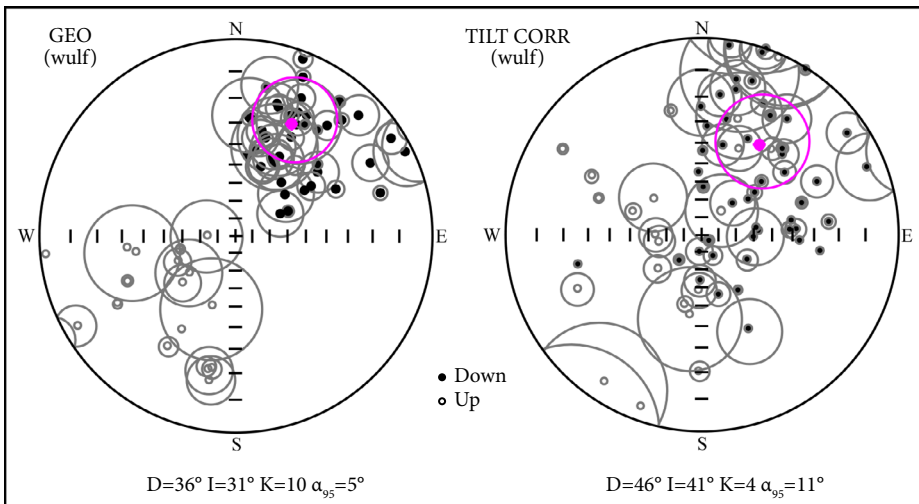


Figure 6. ChRM components. Stereographic projection *in situ* (Geo) and after bedding correction (Tilt Corr).

along the Urica fault (Figure 7A). *In situ*, the site mean direction is easterly deviated ($D = 29^\circ$, $I = 34^\circ$, $k = 22$, $\alpha_{95} = 10^\circ$). The tilt test is here inconclusive because the scattering parameter k is not changing significantly (after bedding correction $D = 162^\circ$, $I = 61^\circ$, $k = 19$, $\alpha_{95} = 11^\circ$). However, the *in situ* declination and inclination are close to the average direction obtained by all ChRMs *in situ* (Figure 5). This observed component was interpreted to have been acquired post-folding and clockwise rotation of $R = 29^\circ \pm 10^\circ$ was calculated (Figure 7). 25Vz, 26Vz and 27Vz sites are located to the north of the Bergantín block, near the El Pilar fault (Figure 9). Cleavage is observed at 27Vz site and strong weathering affects rocks at 25Vz site. *In situ*, the site mean direction is not well defined and strongly easterly deviated ($D = 95^\circ$, $I = 46^\circ$, $k = 7$, $\alpha_{95} = 19^\circ$). After bedding correction, paleomagnetic components seems to scatter ($D = 127^\circ$, $I = 49^\circ$, $k = 5$, $\alpha_{95} = 24^\circ$). Assuming a post-tilting ChRMs and a clockwise rotation of $R = 95^\circ \pm 19^\circ$ (Figure 7B).

4.2.2 Northeast of the San Francisco fault (Caripe block)

This zone is represented by 3Vz, 23Vz and 24Vz sites located to the northwest of the Caripe block, near the San Francisco fault in the SDI (Figure 3). *In situ*, at 3Vz site, the ChRMs yield site mean direction of reverse polarity strongly westerly deviated ($D = 294^\circ$, $I = -21^\circ$, $k = 16$, $\alpha_{95} = 14^\circ$). Bedding correction is inconclusive ($D = 287^\circ$, $I = 34^\circ$, $k = 16$, $\alpha_{95} = 14^\circ$) but deviation of declination is opposite to that observed in the SDI (Figure 7C). Assuming *in situ* data, the rotation observed is $R = 114^\circ \pm 14^\circ$ clockwise. The rocks at 23Vz and 24Vz sites are moderately weathered. These sites were analyzed together,

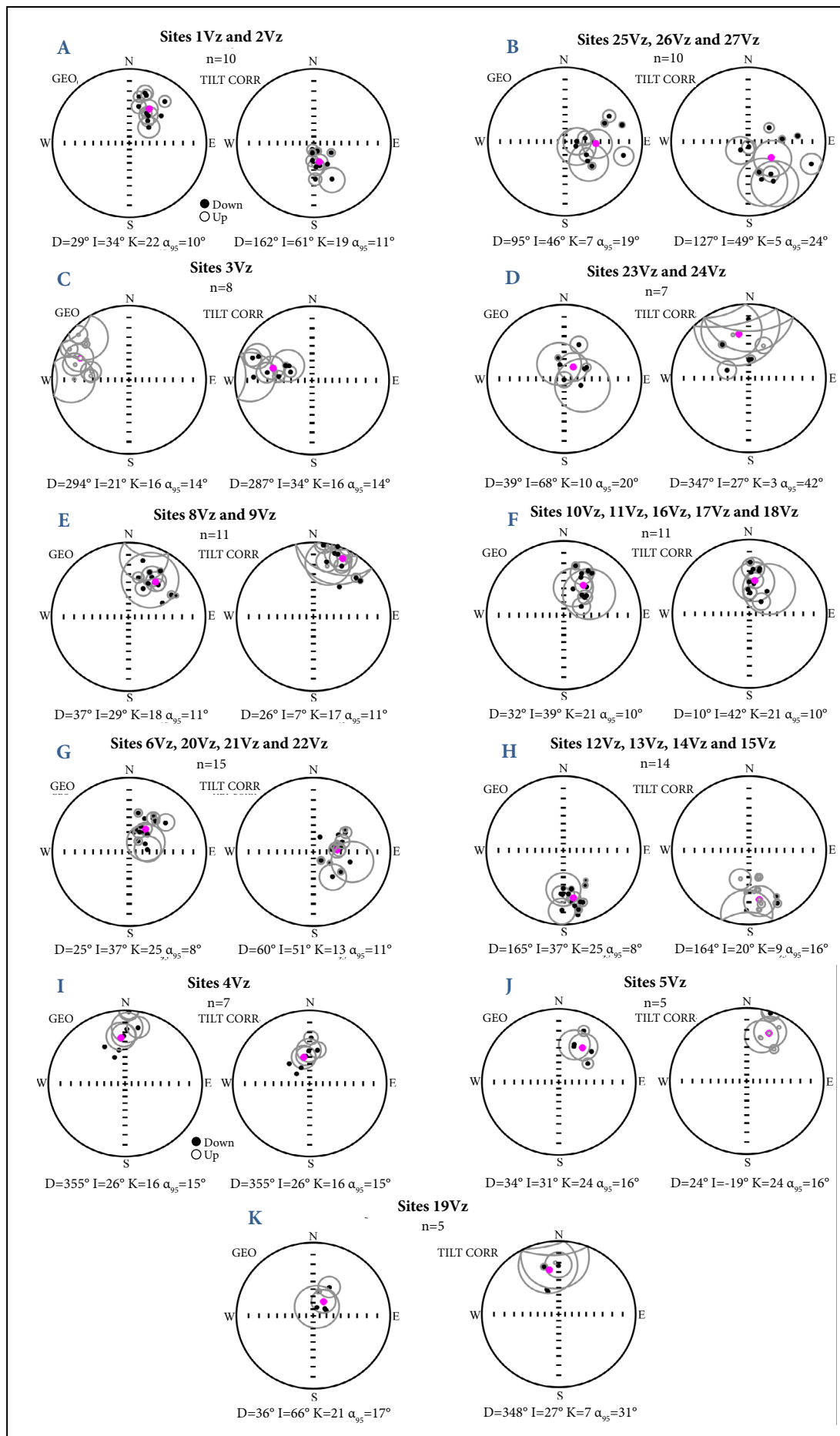


Figure 7. Stereographic projection *in situ* (Geo) and after bedding correction (Tilt) of Component A (ChRM) and Component B.
A and **B**. East of the Urica fault.
C and **D**. Northeast of the San Francisco fault.
E and **F**. South of the San Francisco fault.
G. Center of the Caripe block.
H. East of the Caripe block.
I, J and **K**. were individually interpreted.

yielding a not well defined and steeply inclined site mean direction ($D = 39^\circ$, $I = 68^\circ$, $k = 10$, $\alpha_{95} = 20^\circ$). After bedding correction, the scattering is much more important ($D = 347^\circ$, $I = 27^\circ$, $k = 3$, $\alpha_{95} = 42^\circ$), suggesting post-folding acquisition (Figure 7D). However, inclination is by far too steep ($I = 68^\circ$), and block rotation could not be determined.

4.2.3 South of the San Francisco fault

This zone is represented by 8Vz, 9Vz, 10Vz, 11Vz, 16Vz, 17Vz, and 18Vz sites to the south of the study area near the San Francisco fault (Figure 3). For 8Vz and 9Vz sites located in the Caripe block, *in situ*, the site mean direction is easterly deviated ($D = 37^\circ$, $I = 29^\circ$, $k = 18$, $\alpha_{95} = 11^\circ$) and after bedding correction is inconclusive ($D = 26^\circ$, $I = 7^\circ$, $k = 17$, $\alpha_{95} = 11^\circ$). However, the *in situ* inclination ($I = 29$) is more consistent compared to the inclinations observed in the other studied sites. This magnetization is likely post-folding (Figure 7E). Data suggest a clockwise rotation of $R = 37^\circ \pm 11^\circ$. 10Vz, 11Vz, 16Vz, 17Vz and 18Vz sites are located to the south of the Bergantín block, close the San Francisco fault. *In situ*, the site mean direction is easterly deviated ($D = 32^\circ$, $I = 39^\circ$, $k = 21$, $\alpha_{95} = 10^\circ$) and bedding correction ($D = 10^\circ$, $I = 42^\circ$, $k = 21$, $\alpha_{95} = 10^\circ$) is inconclusive (Figure 7F). This component was interpreted to have been acquired post-folding and clockwise rotation of $R = 32^\circ \pm 10^\circ$ was calculated.

4.2.4 Center of the Caripe block

This zone includes 6Vz, 20Vz, 21Vz and 22Vz sites, all located in the center part of the Caripe block, to the east of the San Francisco fault (Figure 3). *In situ*, the site mean direction of these 4 sites is easterly deviated ($D = 25^\circ$, $I = 37^\circ$, $k = 25$, $\alpha_{95} = 8^\circ$). The orientation of mean direction after bedding correction is less consistent compared to the observed in the other studied sites, because it is steeper ($D = 60^\circ$, $I = 51^\circ$, $k = 13$, $\alpha_{95} = 11^\circ$). Assuming this component post-folding, the block rotation is clockwise and has a magnitude of $R = 25^\circ \pm 8^\circ$ (Figure 7G).

4.2.5 East of the Caripe block

12Vz, 13Vz, 14Vz and 15Vz sites are located on the western edge of the San Juan Graben in the SDI (Figure 3). In this zone, the behavior is totally different from the other zones. *In situ*, the site mean direction of the four sites is of normal polarity and strongly deviated to the south ($D = 165^\circ$, $I = 37^\circ$, $k = 25$, $\alpha_{95} = 8^\circ$). After bedding correction, the mean direction has reverse polarity and correct inclination and declination ($D = 164^\circ$, $I = -20^\circ$, $k = 9$, $\alpha_{95} = 16^\circ$), suggesting pre-tilting acquisition. However, the evolution of the scattering parameter k suggests that the magnetization was acquired post-tilting. If we consider *in situ* data, block rotation is strongly clockwise $R = 165^\circ \pm 8^\circ$, but if we consider tilt correction, the rotation is slightly

counterclockwise ($R = -16^\circ \pm 16^\circ$). We therefore assume that the most reasonable explanation is a pre-tilting magnetization with little or no rotation (Figure 7H).

Finally, 4Vz, 5Vz and 19Vz sites were interpreted individually. 4Vz site is located to the north of the Caripe block, near the El Pilar fault (Figure 3). The calculated *in situ* site mean direction is not deviated ($D = 355^\circ$, $I = 26^\circ$, $k = 16$, $\alpha_{95} = 15^\circ$) and bedding correction is inconclusive ($D = 346^\circ$, $I = 57^\circ$, $k = 12$, $\alpha_{95} = 22^\circ$). According to the observed inclination, this component was interpreted to have been acquired post-folding with a lack of rotation observed (Figure 7I). 5Vz site located to the southeast of 4Vz site in Caripe block, has *in situ* site mean direction easterly deviated ($D = 34^\circ$, $I = 31^\circ$, $k = 24$, $\alpha_{95} = 16^\circ$) and bedding correction is inconclusive ($D = 24^\circ$, $I = -19$, $k = 24$, $\alpha_{95} = 16^\circ$). However, reverse magnetization northerly directed is not likely, and component is post-folding. This suggests clockwise rotation of $R = 34^\circ \pm 16^\circ$ (Figure 7J). 19Vz site is located to the south of the Caripe block (Figure 3). *In situ*, the site mean direction is $D = 36^\circ$, $I = 66^\circ$, $k = 21$, $\alpha_{95} = 17^\circ$ and after bedding correction is $D = 348^\circ$, $I = 27^\circ$, $k = 7$, $\alpha_{95} = 31^\circ$ (Figure 7K). Bedding correction is inconclusive because *in situ* inclination ($I = 66^\circ$) is far too steep compared to the inclinations observed in the other studied sites.

5. Discussion

5.1 Regional analysis of paleomagnetic data

A regional paleomagnetic study was carried out at 26 of the 27 sampled sites in the SDI, except for 7Vz site which showed an unstable and uninterpretable demagnetization track. A VRM is present in 23% of the specimens of the sites (Table 2), yielding a rather steep inclination on average ($I = \sim 35^\circ$), consistent with the present day's earth magnetic field. This inclination is steeper by $\sim 15^\circ$ with respect to the GAD and by $\sim 24^\circ$ with respect to the APWP_{0-10Ma}. Thus, it is possible that this abnormally high inclination has existed in this area for several Ma. A characteristic remanent magnetization (ChRM) is present in 63% of the site specimens (Table 2). According to the bedding-tilt test, the ChRM present in the SDI was essentially acquired post-folding (Figure 5).

From the analysis of different sub-groups, four main behaviors with respect to the inclination and declination obtained were observed (Table 3, Figures 8 and 9).

5.1.1 Group analysis according paleomagnetic results

Group 1 includes 13 sites (Table 3) and shows the regional paleomagnetic behavior of the SDI. This group allows us to define the timing of remagnetization and the regional block rotation sense. Both magnetic polarities are observed in this group, of which $\sim 30\%$ are reverse. *In situ*, the mean direction

Table 3. Paleomagnetic result organized by groups

Group	Sites	Samples analyzed	Geo				Tecto (Tilt Corr)			
			D	I	K	α_{95}	D	I	K	α_{95}
1	1Vz, 2Vz, 5Vz, 6Vz, 8Vz, 9Vz, 10Vz, 11Vz, 16Vz, 17Vz, 18Vz, 20Vz, 21Vz, 22Vz	98 (118)	37	31	12	4	36	31	9	9
2	3Vz, 25Vz, 26Vz, 27Vz	19(29)	105	35	8	13	291	10	3	26
3	12Vz, 13Vz, 14Vz, 5Vz	12	163	37	24	10	344	21	9	16
4	19Vz, 23Vz, 24Vz	11(24)	33	68	12	13	344	31	5	22

is easterly deviated ($D = 37^\circ$, $I = 31^\circ$, $k = 12$, $\alpha_{95} = 4^\circ$). After bedding correction, declination is equally easterly deviated ($D = 36^\circ$, $I = 34^\circ$, $k = 4$, $\alpha_{95} = 9^\circ$) and larger scattering confirms the post tilting origin (Figures 9 and 10). This is therefore a remagnetization. Group 1 suggests a regional clockwise block rotation of $R = 37^\circ \pm 4^\circ$ both in the Bergantin block and Caripe block (Figures 8 and 9).

Group 2 includes 5 sites (Table 3), all located to the north of the SDI near the El Pilar strike-slip fault. The components are essentially reverse (11 of 18) and relatively scattered. *In situ*, the site mean direction is strongly deviated ($D = 135^\circ$, $I = 35^\circ$, $k = 8$ and $\alpha_{95} = 13^\circ$) and the bedding-tilt test suggests a

post-folding acquisition, like the sites from Group 2 (Figure 8). The declination *in situ* suggests a clockwise block rotation of $R = 105^\circ \pm 13^\circ$ (Figures 8 and 9). High magnitudes of block rotation ($> 90^\circ$) are sometimes observed in fold and thrust belts as the Betics [45] or the Alps [46], but this is rather exceptional. High magnitude clockwise block rotation from 107° to 207° was documented within the core of the north Anatolian fault [47]. It is therefore possible that paleomagnetic components of this group might be related to the core of the strike-slip fault zone. Additionally, these sites are observed to be aligned E-W, supporting the presence of a possible strike-slip fault within the boundary of the El Pilar fault system.

Group 3 includes 4 sites (Table 3) located to the east of the SDI, at the western boundary of the San Juan Graben. All components display *in situ* normal polarity. The *in situ* site mean direction of Group 3 is strongly deviated ($D = 163^\circ$, $I = 37^\circ$, $k = 24$, $\alpha_{95} = 10^\circ$) and after bedding correction, the reverse component is much closer to the reference direction ($D = 164^\circ$, $I = -20^\circ$, $k = 9$, $\alpha_{95} = 16^\circ$) (Figure 8). The bedding-tilt test shows that magnetization directions are more clustered before bedding correction ($k = 25$), suggesting that the remagnetization was acquired post-folding. However, the declination and inclination after bedding correction are close to the present day's EMF. *In situ*, block rotation is strongly clockwise $R = 163^\circ \pm 10$. After bedding correction, the rotation is slightly counterclockwise ($R = -16^\circ \pm 16^\circ$) (Figure 8). Here, the most reasonable solution is assumed to be that the paleomagnetic component of Group 3 is likely a pre-folding magnetization with little or no rotation. This hypothesis must be confirmed by further studies due to the lack of significant rotation along the boundary of the San Juan Graben, delineating a possible block limit.

Group 4 includes 19Vz site located in the Caripe block and 23Vz and 24Vz sites located to the north of the Serranía, near the San Francisco fault. All components have normal polarity and *in situ* site mean direction is easterly deviated and is steeply inclined ($D = 33^\circ$, $I = 68^\circ$, $k = 12$, $\alpha_{95} = 13^\circ$). Inclination is becoming more consistent after bedding correction, but scatter increases ($D = 344^\circ$, $I = 31^\circ$, $k = 5$, $\alpha_{95} = 22^\circ$). The bedding-

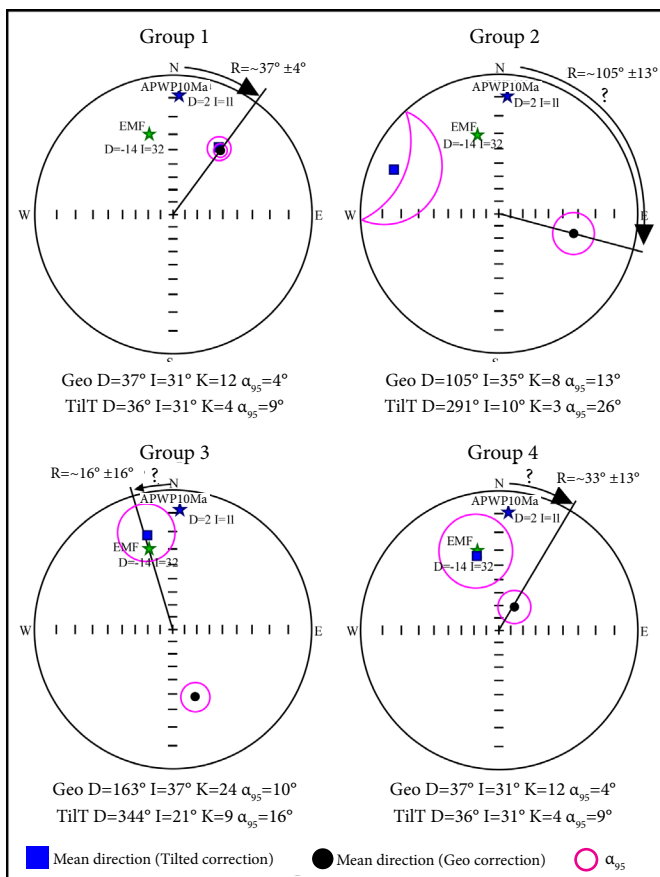


Figure 8. Paleomagnetic statics results obtained for Groups 1, 2, 3 and 4. For clarity, all mean vectors are plotted with normal polarities.

tilt test shows a more clustered magnetization direction before bedding correction, suggesting that the remagnetization was acquired post-folding. The *in situ* declination indicates clockwise block rotation of $R = 33^\circ \pm 13^\circ$ (Figure 8). This group is characterized by a very steep inclination of 68° . More sampling in the zone is necessary in order to confirm and to understand this behavior.

To sum up, Groups 1, 2, and 4 reveal a post-folding remagnetization, only Group 3 is potentially pre-tilting. Groups 1 and 4 reveal a large dominance of clockwise rotation of $\sim 35^\circ$. Group 2, if confirmed, displays the strongest clockwise deviation up to $\sim 100^\circ$.

5.2 Timing of the remagnetization and block rotation in the SDI

The SDI is the hinterland of the orogenic prism formed as a consequence of the interaction between the Caribbean and the South American plates. Based on fission track data, the main folding stage of the SDI stopped at 12 Ma [32] and according to tectonic plate reconstruction, this happened at 10 Ma [31, 28, 24]. Thus, regional post folding remagnetization (Group 1) is younger than $\sim 10 - 12$ Ma. Post-folding remagnetization is a common process observed in many thrusts and belts, and particularly, within the hinterland of the thrust belt. An example of the magnetization relative to the folding pattern was studied in the central Appalachians [48]. In that model, the timing of the magnetization is associated with the sequence of deformation propagating from the hinterland to the foreland basin. Post-folding remagnetization is observed in the hinterland where folds were formed before remagnetization, then in the foothills (central part of the belt) the remagnetization is synfolding because folds were developed during the remagnetization and finally, pre-folding remagnetization is observed near the

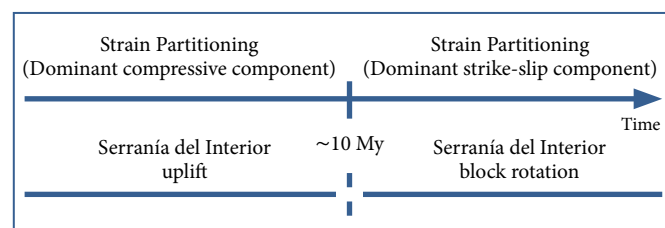


Figure 9. Scheme showing a strain partitioning state in the SDI before and after ~ 10 Ma.

foreland basin where folds developed after remagnetization. It is possible that the remagnetization observed in the SDI hinterland obeys the same pattern.

The remagnetization observed in Groups 1, 2 and 3 was acquired after 10-12 Ma, and at that time, the strike-slip component dominated in eastern Venezuela [31, 28, 24]. As a result, the deformation in the foreland basin decreased considerably. Based on this, we suggest that the regional clockwise block rotation of $R = 37^\circ \pm 4^\circ$ observed in the SDI is synchronous with the dominant right-lateral strike-slip component (Figure 9). Taking an age ~ 10 Ma as the minimum age of the block rotation (post-folding period), a minimum rotation rate of $3.7^\circ/\text{Ma}$ was estimated.

5.3 Integration with previous paleomagnetism studies

In Northern Venezuelan there are very few paleomagnetic studies and these studies lack tilt test. Skerlec and Hargraves [49] worked on the northwest Venezuelan Basin and detected a large clockwise rotation of the paleomagnetic component; however, they neither report its magnitude nor discuss the bedding tests. Burmester [50] studied volcanic and metavolcanic rocks from the island of Tobago showing a pre-tilting component and a strong clockwise deviation. The results of our work are therefore consistent with these two studies along the southern

boundary of the Caribbean plate, where large clockwise rotations of about 90° were detected. Similarly, Reid [51] reported in Puerto Rico a post-Late Miocene (between 11 and 4.5 Ma) counterclockwise rotation of $25^\circ \pm 6^\circ$ and a rotation rate of $4^\circ/\text{Ma}$ was inferred. In central Cuba, Tait [52] reported pre- to syn-tilting magnetization and strong counterclockwise rotation. The broad picture of the paleomagnetic results is clockwise rotation in the southern Caribbean boundary and counterclockwise rotation in the northern Caribbean boundary (Figure 10). This picture closely

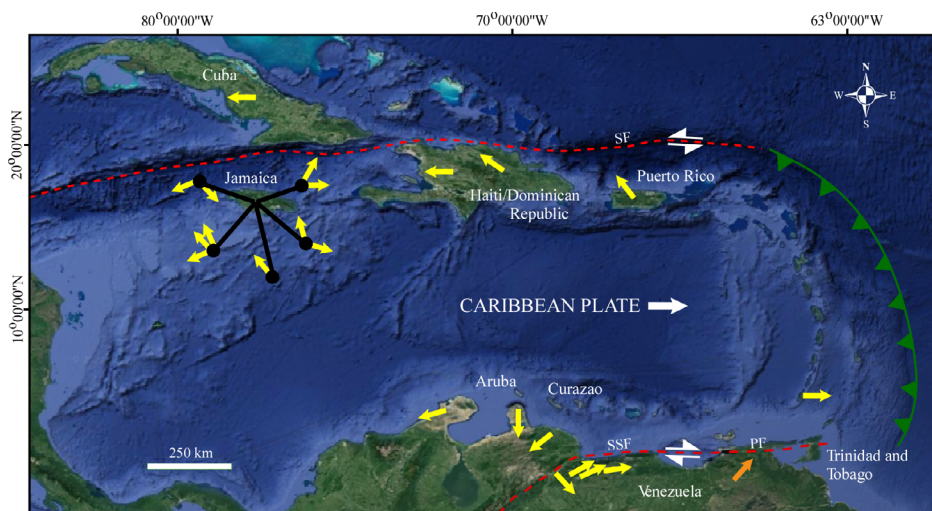


Figure 10. Caribbean map showing the rotation direction along the southern and northern boundaries of the Caribbean plate. The yellow arrows represent paleomagnetic data compiled by [48, 50, 51]. The orange arrow represents the paleomagnetic data obtained in this study. SF = Septentrional Fault, BF = Boconó Fault, SSF = San Sebastián Fault, PF = El Pilar Fault.

resembles the block rotation observed in the Betic-Rif Arc [45].

5.4 Relation between strike-slip faulting and block rotation in the SDI and MFTB

There are several conceptual models to explain block rotation in strike-slip regimes: domino-shaped blocks with heterogeneous blocks [54], only lateral displacement of blocks accommodated the strike-slip movement and lack of significant rotation [55], counterclockwise block rotation in a right lateral regime [56], and strain model with strain partitioning and strain distribution in the whole area [57]. However, the SDI does not possess the configuration that these models present, as for example, a major strike-slip faulting in the south. Other authors have proposed relating strike-slip motion to synthetic Riedel shear formation but without mentioning block rotation associated with this system [15]. For this reason, we propose relating the structural configuration of the SDI to the analogue model developed by Schreurs [58], which shows that the displacement of a major dextral strike-slip fault develops oblique dextral strike-slip synthetic Riedel shear and thus, clockwise block rotation.

In agreement with Schreurs model, the synthetic Riedel shear system in the SDI is represented by the El Pilar fault as the master regional strike-slip fault and by the Urica and San Francisco faults as synthetic Riedel shears. This faults system is associated with a clockwise block rotation of $37^\circ \pm 4^\circ$ during the last ~ 10 Ma ($3.7^\circ/\text{Ma}$) measured by the paleomagnetic data in both the Caribe and Bergantín blocks. Also, it is observed that the rotation of the smaller blocks [58] can vary but the regional rotation sense will be the same. Similarly, in the SDI rotation values that vary from 16° near the San Juan Graben up to 105° near the El Pilar fault and all sense of rotation is always clockwise (Figure 3).

5.5 Active deformation in the SDI and the MFTB

The clockwise rotation inferred from paleomagnetic data is consistent with a Riedel system model, represented by the Urica and San Francisco faults, in response to the El Pilar fault dextral movement. We further develop this synthetic Riedel shear model by proposing that part of the SDI movement is accommodated towards the south, specifically in the MFTB where evidences for active compression are topographic uplifts, deformed terraces, drainage anomalies, reactivation of old thrusts formed during the middle Miocene (e.g. the Pirital and Tarragona thrusts) [18]. Cosmogenic dating of river terraces in the MFTB shows that these were exposed during the late Pleistocene. The oldest terrace, located in the Tarragona zone, has an exposure age of ~ 90 ka, and the youngest, located in the Punta de Mata zone, an exposure age of ~ 15 ka. Regarding the

vertical deformation rates, the highest rates are observed near the Urica fault, at the Tarragona Ridge 0.33 ± 0.06 mm/y and Amarilis Ridge 0.6 ± 0.2 mm/y [18]; whereas, far from the fault, to the east, the vertical rates decrease to ~ 0.1 mm/y in the Pirital and Jusepín zones, additionally seismic data shows that the deformation observed in the MFTB is located just above deep structures related to the Tarragona, Pirital, Furrial thrusts and the Amarilis backthrust, terrace dating and seismic interpretation indicate that deformation in the MFTB is an ongoing process [18]. All these thrusts and topographic ridges are a consequence of the Urica fault horsetail terminations as a part of the Riedel shear system movement developed in the SDI after ~ 11 Ma to the present day [18].

5.6 Neogene geodynamic model for Northeastern Venezuela

The geodynamics in Northeastern Venezuela from the Miocene to the present have evolved in different ways throughout the region. On the basis of our results and the previous studies carried out by several authors in the area, an evolutionary tectonics model of the SDI and MFTB is proposed as follows:

- From 20 to 12 Ma (early-middle Miocene): Active uplifting of the SDI hinterland from the middle Eocene around 45 Ma [32, 59]. At 12 Ma: The SDI uplift stopped [32, 60]. Onset of strain partitioning in the area [60].
- From 12 to 5.3 Ma (late Miocene): Strain partitioning continued but wrenching is the dominant component in the area up to present. The El Pilar strike-slip fault movement develops the Urica and San Francisco synthetic Riedel shears and then block rotation begins. The Urica fault dextral movement develops thrusts at its tip end (horsetail termination) forming the Tarragona, Pirital and Furrial thrusts. Thus, the Urica fault movement accommodates part of the Caribbean and South American plate interaction within the MFTB, resulting in the out-of-sequence reactivation of the Pirital thrust. The reactivation of the Pirital thrust has been proposed by several authors [61, 8, 62]. In the present study, we also propose not only a reactivation of this thrust, but also a reactivation of the Tarragona thrust (Figure 11).
- From ~ 5.3 to 0 Ma (Pliocene to the present day): block rotation in the SDI and thrusting in the MFTB prevail up to present day. In addition, NW-SE normal faults are developed at this time. These normal faults that form the San Juan Graben in the SDI were possibly formed by the transtension to the east since the Pleistocene, as reported by [5]. This same transtension formed the

Gulf of Paria pull-apart in the Pleistocene [63, 64]. 3) The most important post-middle Miocene deformation is being developed to the south of the MFTB during this time with an uplift rate ≤ 0.6 mm/y and a shortening to the west of ~ 1.3 km which decrease to ~ 0.5 km to the east (Figure 11).

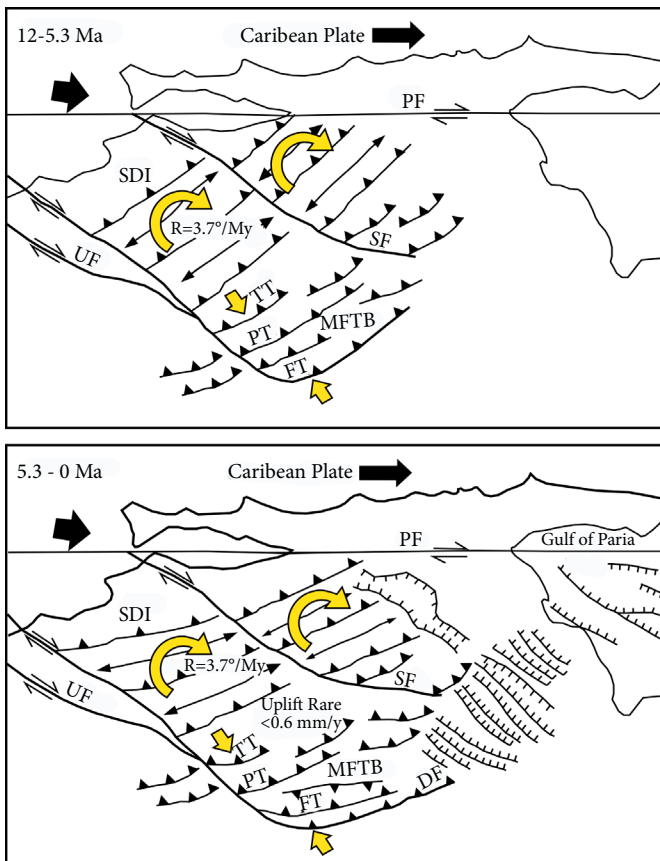


Figure 11. Tectonic and structural evolution of the SDI and MFTB from ~ 12 to 5.3 Ma. SDI: Serranía del Interior, MFTB: Monagas Fold and Thrust Belt, PF: Pilar Fault, UF: Urica Fault, SSF: San Francisco Fault, TT: Tarragona Thrust, PT: Pirital Thrust, FT: Furrial Thrust, DF: Deformation Front. Normal faults were compiled from [7].

6. Conclusions

This work is the first paleomagnetic study carried out in the Serranía del Interior (SDI). This exploratory survey shows unambiguously that a pervasive post-folding remagnetization occurred in the SDI hinterland. As the folding stopped due to a major change of the El Pilar fault movement around 11 Ma ago, the paleomagnetic component thus provides information about tectonic events younger than 11 Ma. Four groups were identified: three groups that gathers post-folding remagnetization, and one group that is compatible with pre-folding remagnetization. Group 1 (1Vz, 2Vz, 5Vz, 6Vz, 8Vz, 9Vz, 10Vz, 11Vz, 16Vz, 17Vz, 18Vz, 20Vz, 21Vz and 22Vz sites) by far the most important one, displaying a regional clockwise block rotation along vertical axis of $37^\circ \pm 4^\circ$ (average rotation rate of $\sim 3.7^\circ/\text{Ma}$). Group 4 (19Vz, 23Vz and 24Vz

sites) also suggests a similar clockwise rotation of $33^\circ \pm 13^\circ$, however, this paleomagnetic component is characterized by a very steep inclination of $\sim 68^\circ$. Group 2 (3Vz, 25Vz, 26Vz and 27Vz sites) displays unusually large clockwise rotation of $105^\circ \pm 13^\circ$. We suggest that such a rotation is related to a blind segment of El Pilar fault system. Group 3 (12Vz, 13Vz, 14Vz and 15Vz sites), located within the eastern part of the studied area, shows a pre-folding remagnetization and displays a slightly counterclockwise rotation ($R = -16^\circ \pm 16^\circ$). We propose a Neogene geodynamic model of the SDI and MFTB. In the SDI, the Urica and San Francisco dextral faults are considered as synthetic Riedel shears of the El Pilar fault created around ~ 12 Ma. From 12 to 0 Ma, the Riedel faults activity caused clockwise block rotation of $\sim 37^\circ$ in the Caripe and Bergantín blocks. From 5.3 to 0 Ma, NW-SE normal faults were developed forming the San Juan Graben in the SDI and the Gulf of Paria pull-apart due to transtension to the east (Figure 11). To the south of the MFTB, another deformation phase is being developed that is active up to the present day, forming Pleistocene terraces, topographic uplifts and also reactivating the old thrusts of this area.

7. Acknowledgments

This work is part of Atiria Fajardo's Ph.D. research at the Université de Pau et des Pays de l'Adour, France. Atiria Fajardo wants to thank Fundación Gran Mariscal de Ayacucho (FUNDAYACUCHO), French Embassy in Venezuela, Université de Pau et des Pays de l'Adour and Petróleos de Venezuela, S.A. (PDVSA) for partially supporting AF research. The authors would like to thank Damien Dhont, who participated in the initiation of the project, Yves Hervouet and Jean-Paul Xavier for supporting its development. We are also grateful to Dr. Frances McCarty, to the reviewers and editors who improved this paper with their comments and suggestions.

References

- [1] Ross, M. I., and Scotese, C. R. A hierarchical tectonic model of the Gulf of Mexico and Caribbean region. *Tectonophysics*, **155**(1), 139-168 (1988).
- [2] Meschede, M., and Frisch, W. A plate-tectonic model for the Mesozoic and Early Cenozoic history of the Caribbean plate. *Tectonophysics*, **296**(3), 269-291 (1998).
- [3] Stephan, J., De Lepinay, B., M., Calais, E., Tardy, M., Beck, C., Carfantan, J., Olivet, J., L., Vila, J., M., Bouysse, P., Mauffret, A., Borgo, J., Thery, J., M., Tournon, J., Blanchet, and R., Dercourt, J. Paleogeodynamic maps of the Caribbean: 14 steps from Lias to present. *Bull. Soc. Géol. France*, **8**(9), 281-282 (1990).
- [4] Mann, P. Caribbean sedimentary basins: classification and tectonic setting from Jurassic to present. In: Mann, P. (ed.), *Caribbean Basins. Sedimentary Basins of the World*, vol. 4. Elsevier Science B.V., Amsterdam, (1999) pp. 3-31.

- [5] Pindell, J. L., Kennan, L., Wright, and D., Erikson, J. Clastic domains of sandstones in central/eastern Venezuela, Trinidad, and Barbados: heavy mineral and tectonic constraints on provenance and palaeogeography. In: James, K. H., Lorente, M. A. and Pindell, J. L. (Eds.) *The Origin and Evolution of the Caribbean plate*. Geological Society, London, *Special Publications*, **328**, 743–797 (2009).
- [6] Roure, F., Bordas-Lefloch, N., Toro, J., Aubourg, C., Guilhaumou, N., Hernandez, E., Lecornec-Lance, S., Rivero, C., Robion, and P., Sassi, W. Reservoir Appraisal in the Sub-Andean Basins (Eastern Venezuela and Eastern Colombian Foothills). In: RTB in C. Bartolini and J. Blickwede (eds). *The Circum-Gulf of Mexico and the Caribbean: Hydrocarbon habitats, basin formation, and plate tectonics*. American Association of Petroleum Geologists (2003) pp. 750-775.
- [7] Duerto, L. Shale tectonics, eastern Venezuelan basin (Doctoral dissertation, Royal Holloway, University of London, 2007).
- [8] Parra, M., Sánchez, G. J., Montilla, L., Guzmán, O. J., Namson, J., and Jácome, M. I. The Monagas Fold-Thrust Belt of Eastern Venezuela. Part I: Structural and thermal modeling. *Marine and Petroleum Geology*, **28**(1), 40-69 (2011).
- [9] Garrity C., Hackley, P.C., and Urbani, F. Digital geological map and GIS database of Venezuela. U.S. G. S., Data Series 199 (<http://pubs.usgs.gov/ds/2006/199/>), 2006.
- [10] Zinck, J. A. and Urriola, P. L. Origen y evolución de la Formación Mesa. Un enfoque edafológico. Barcelona, Venezuela: Ministerio de Obras Públicas (MOP, 1970).
- [11] Singer, A., Beltrán C., and Rodríguez, J. A. Evidencias geomorfológicas de actividad neotectónica a lo largo de los corrimientos frontales de la Serranía del Interior en el oriente venezilano. *3rd. Geological Conference of the Geological Survey of Trinidad and Tobago* (1995).
- [12] Audemard, F. A., Machette, M., Cox, J., Dart, R. and Haller, K. Map and Database of Quaternary Faults and Folds in Venezuela and its Offshore Regions. USGS Open-File report 00-0018, 2002. (accesible from USGS webpage: <http://greenwood.cr.usgs.gov/pub/open-file-reports/ofr-00-0018>).
- [13] Wagner, R. Estudio estructural regional y análisis de deformaciones recientes en el frente de montaña de La Serranía Del Interior Oriental y en la parte Norte de la Subcuenca de Maturín. Unpublished undergraduate work, Universidad Central de Venezuela, Caracas, Venezuela (2004).
- [14] Fajardo, A. Neotectonic evolution of the Serranía del Interior range and Monagas Fold and Thrust belt, Eastern Venezuela: morphotectonics, seismic profiles analyses and paleomagnetism. (Doctoral dissertation, University of Pau, France, 2015).
- [15] Audemard, F., Romero, G., Rendon, H., and Cano, V. Quaternary fault kinematics and stress tensors along the southern Caribbean from fault-slip data and focal mechanism solutions. *Earth-Science Reviews* **69**, 181–233 (2005).
- [16] Jouanne, F., Audemard, F. A., Beck, C., Van Welden, A., Ollarves, R., and Reinoza, C. Present-day deformation along the El Pilar Fault in eastern Venezuela: Evidence of creep along a major transform boundary. *Journal of Geodynamics*, **51**(5), 398-410 (2011).
- [17] Reinoza, C., Jouanne, F., Audemard, F. A., Schmitz, M., and Beck, C. Geodetic exploration of strain along the El Pilar Fault in northeastern Venezuela. *Journal of Geophysical Research: Solid Earth*, **120**(3), 1993-2013 (2015).
- [18] Fajardo, A., Aubourg, C., Niviere, B., Regard, V. and Uzcátegui, R. Geomorphological and seismic analysis in the Monagas Fold and Thrust Belt. *Journal of South American Earth Sciences* **104**, 10267 (2020). <https://doi.org/10.1016/j.jsames.2020.102867>.
- [19] Eva, A. N., Burke, K., Mann, P., and Wadge, G. Four-phase tectonostratigraphic development of the southern Caribbean. *Marine and Petroleum Geology*, **6**(1), 9-21 (1989).
- [20] Parnaud, F., Gou, Y., Pascual, J.-C., Truskowski, I., Gallango, O., Passalacqua, H. and Roure, F. Petroleum geology of the central part of the Eastern Venezuela basin. In A. J. Tankard, R. Suárez S. and H. J. Welsink (Eds.) *Petroleum basins of South America: AAPG Memoir* **62**, 741–756 (1995).
- [21] Pindell, J. L. and Barrett, S. F. Geological evolution of the Caribbean region: a plate tectonic perspective. In Dengo, G. and Case, J. E. (Eds.), *The Geology of North America, The Caribbean Region*, *Geological Society of America*, V.(H), 405-432 (1990)..
- [22] Passalacqua, H., Fernandez F., Gou, Y. and Roure, F. Crustal architecture and strain partitioning in the eastern Venezuelan Ranges. In Tankard, A. J., Suárez, S. R., and Welsink, H. J., *Petroleum basins of South America: AAPG Memoir* **62**, 667–679 (1995).
- [23] Avé Lallement, H. G. Transpression, displacement partitioning, and exhumation in the eastern Caribbean/South American plate boundary zone. *Tectonics*, **16**(2), 272-289 (1997).
- [24] Lingrey, S. Plate tectonic setting and cenozoic deformation of Trinidad: fold belt restoration in a region of significant strike-slip. In *Thrust Belts and Foreland Basins*. (Springer Berlin Heidelberg 2007) pp. 163-178.
- [25] Dolan, J., Mann, P., Preface. In: Dolan, J., and Mann, P. (Eds.), Active strike-slip and collisional tectonics of the Northern Caribbean plate boundary, *The Geological Society of America*, **326** (1998) pp. v-xvi.
- [26] DeMets, C., Jansma P. E., Mattioli G. S., Dixon T. H., Farina F., Bilham R. Calais E and Mann P. GPS geodetic constraints on Caribbean-North America plate movement. *Geophys. Res. Lett.*, **27**(3), 437-440 (2000).
- [27] Pérez, O. J., Bilham, R., Bendick, R., Velandia, J. R., Hernández, N., Moncayo, C., Hoyer, M. and Kozuch, M. Velocity field across the southern Caribbean plate boundary and estimates of Caribbean/South-American plate movement using GPS geodesy 1994-2000 (Paper 2001GL013183). *Geophysical Research Letters*, **28**(15), 2987-2990 (2001).
- [28] Weber, J. C., Dixon, T. H., DeMets, C., Ambeh, W. B., Jansma, P., Mattioli, G., Saleh, J., Sella, G., RBilham, R., and Pérez, O.). GPS estimate of relative movement between the Caribbean and South American plates, and geologic implications for Trinidad and Venezuela. *Geology*, **29**(1), 75-78 (2001).
- [29] Pérez, O. J., Wesnousky, S. G., De La Rosa, R., Marquez, J., Uzcátegui, R., Quintero, C., Liberal, L., Mora-Páez, H., and Szeliga, W. On the interaction of the North Andes plate with the

- Caribbean and South American plates in northwestern South America from GPS geodesy and seismic data. *Geophys. J. Int.*, **214**, 1986–2001 (2018).
- [30] Algar, S., and Pindell, J. Structure and deformation history of the northern range of Trinidad and adjacent areas: *Tectonics*, **12**, 814-829 (1993).
- [31] Pindell J., Higgs, R. and Dewey J. Cenozoic palinspastic reconstruction, paleogeographic evolution and hydrocarbon setting of the northern margin of South America. *SEPM Special Publication*, **58**, 45-85 (1998).
- [32] Locke, B. D., and Garver, J. I. Thermal evolution of the eastern Serranía del Interior foreland fold and thrust belt, northeastern Venezuela, based on apatite fission-track analyses. *Geological Society of America Special Papers*, **394**, 315-328 (2005).
- [33] Ysaccis, R. Tertiary Evolution of the Venezuelan Northeastern Offshore (Doctoral dissertation, PhD Thesis, Rice University, Houston, 1997).
- [34] Di Croce, J., Bally, A.W., and Vail, P, Sequence stratigraphy of the Eastern Venezuelan Basin. In: Mann, P. (Ed.), *Caribbean Basins. Sedimentary Basins of the World*, **4**. Elsevier Science B.V, Amsterdam, The Netherlands, pp. 419–476 (1999) pp. 419-176.
- [35] Audemard, F. A., Singer, A., and Soulás, J. P., FUNVISIS Neotectonics Section. Quaternary faults and stress regime of Venezuela. *Revista de la Asociación Geológica Argentina*, **61**, 480-461 (2006).
- [36] Ysaccis, R., Cabrera, E. y Del Castillo, H. El sistema petrolífero de la cuenca de la Blanquilla, costa afuera Venezuela. *VII Simposio Bolivariano Exploración Petrolera en las Cuencas Subandinas*, Caracas, (2000), pp. 411-425.
- [37] Rosales, H. La falla de San Francisco en el Oriente de Venezuela. *Boletín de Geología, Publicación Especial*, **5**, 2322-2336 (1972).
- [38] Chaplet, M. Área Cerro Corazón – Anticlinal Punceres (Prolongamiento oriental de la fosa de Espino) Complemento geológico del estudio: Dominio de la Serranía del Interior Oriental y su Cuenca Molásica. *PDVSA Internal Report* (2002).
- [39] Rossi, T. Contribution à l'étude géologique de la frontière Sud-Est de la plaque Caraïbes: La Serranía Del Interior Oriental (Venezuela) sur le transect Cariaco-Maturín (Doctoral dissertation, 1985).
- [40] Cogné, J.P. PaleoMac: A Macintosh™ application for treating paleomagnetic data and making plate reconstructions. *AGU and the Geochemical Society*, **4**(1), 1007. doi:10.1029/2001GC000227, 2003.
- [41] Tauxe, L., Banerjee, S. K., Butler, R. F. and Van der Voo, R.. Essentials of Paleomagnetism, 5th Web Edition. (2018).
- [42] Fisher, N. I., Lewis, T. and Embleton. B. J. *Statistical analysis of spherical data*. Cambridge, UK Cambridge University Press. (1987) pp. 343.
- [43] Besse, J., and Courtillot, V. Apparent and true polar wander and the geometry of the geomagnetic field over the last 200 Ma. *Journal of Geophysical Research: Solid Earth* (1978–2012), **107**(B11), EPM-6 (2002).
- [44] Garrity C., Hackley, P. C., and Urbani, F. Digital shaded relief map of Venezuela. U. S. G. S. Open-File Report 2004-1322, scale 1:1.500.000 (<http://pubs.usgs.gov/>)
- [45] Platt, J. P., Allerton, S., Kirker, A., Mandeville, C., Mayfield, A., Platzman, E. S., and Rimi, A. The ultimate arc: Differential displacement, oroclinal bending, and vertical axis rotation in the External Betic-Rif arc. *Tectonics*, **22**(3) (2003).
- [46] Collombet, M., Thomas, J.C., Chauvin, A., Tricart, P., Bouillin, J.P., and Gratier, J.P. Counterclockwise rotation of the western Alps since the Oligocene: New insights from paleomagnetic data. *Tectonics*, **21**(4), 14-1 (2002).
- [47] Piper, J. D. A., and Rui, Z. Q. Palaeomagnetism of Neoproterozoic glacial rocks of the Huabei shield: the North China block in Gondwana. *Tectonophysics*, **283**(1), 145-171 (1997).
- [48] Stamatakos, J., Hirt, A. M., and Lowrie, W. The age and timing of folding in the central Appalachians from paleomagnetic results. *Geological Society of America Bulletin*, **108**(7), 815-829 (1996).
- [49] Skerlec, G. M., and Hargraves, R.B. Tectonic significance of paleomagnetic data from northern Venezuela. *Journal of Geophysical Research: Solid Earth* (1978–2012), **85**(B10), 5303-5315 (1980).
- [50] Burmester, R. F., Beck, M. E., Speed, R. C., and Snoke, A. W. A preliminary paleomagnetic pole for mid-Cretaceous rocks from Tobago: further evidence for large clockwise rotations in the Caribbean-South American plate boundary zone. *Earth and Planetary Science Letters*, **139**(1), 79-90 (1996).
- [51] Reid, J. A., Plumley, P. W., and Schellekens, J. H. Paleomagnetic evidence for late Miocene counterclockwise rotation of north coast carbonate sequence, Puerto Rico. *Geophysical Research Letters*, **18**(3), 565-568. (1991).
- [52] Tait, J., Rojas-Agramonte, Y., García-Delgado, D., Kröner, A., and Pérez-Aragón, R. Palaeomagnetism of the central Cuban Cretaceous Arc sequences and geodynamic implications. *Tectonophysics*, **470**(3), 284-297 (2009).
- [53] Google (2021). Caribbean Sea. Available at: <https://earth.google.com/web/@15.19026138,-70.59306812,-81731.38827871a,1851885.44800669d,35y,0h,0t,0r>. (Accessed: 18 November 2022).
- [54] McKenzie, D., and Jackson, J. The relation between strain rates, crustal thickening, palaeomagnetism, finite strain and fault movements within a deforming zone. *Earth and Planetary Science Letters*, **65**(1), 182-202 (1983).
- [55] Geissman, J. W., Callian, J. T., Oldow, J. S., and Humphries, S. E. Paleomagnetic assessment of oroflexural deformation in west-central Nevada and significance for emplacement of allochthonous assemblages. *Tectonics*, **3**(2), 179-200 (1984).
- [56] Garfunkel, Z., Zak, I., and Freund, R. Active faulting in the Dead Sea rift. *Tectonophysics*, **80**(1), 1-26 (1981).
- [57] Canérot, J., Hudec, M. R., and Rockenbauch, K. Mesozoic diapirism in the Pyrenean orogen: salt tectonics on a transform plate boundary. *AAPG Bulletin*, **89**(2), 211-229 (2005).
- [58] Schreurs, G. Experiments on strike-slip faulting and block rotation, *Geology*, **22**, 567-570 (1994).

- [59] Sisson, V., Avé Lallement, H. G., Ostos, M., Blythe, A., Snee, L., Copeland, P., Wright, J., Donelick, R., and Guth, L. Overview of radiometric ages in three allochthonous belts of northern Venezuela: Old ones, new ones, and their impact on regional geology. *Geological Society of America Special Papers*, **394**, 91-117 (2005).
- [60] Escalona, A., and Mann, P. Tectonics, basin subsidence mechanisms, and paleogeography of the Caribbean-South American plate boundary zone. *Marine and Petroleum Geology*, **28**(1), 8-39 (2011).
- [61] Roure, F., Carnevali, J. O., Gou, Y., and Subieta, T. Geometry and kinematics of the North Monagas thrust belt (Venezuela). *Marine and Petroleum Geology*, **11**(3), 347-362 (1994).
- [62] Salazar, M., Moscardelli, L., Fisher, W., and Lorente, M. A. Tectonostratigraphic evolution of the Morichito piggyback basin, Eastern Venezuelan Basin. *Marine and Petroleum Geology*, **28**(1), 109-125 (2011).
- [63] Babb, S., and Mann, P. Structural and sedimentary development of a Neogene transpressional plate boundary between the Caribbean and South America plates in Trinidad and the Gulf of Paria. *Sedimentary Basins of the World*, **4**, 495-557 (1999).
- [64] Flinch, J. F., Rambaran, V., Ali, W., De Lisa, V., Hernandez, G., Rodrigues, K., and Sams, R. Structure of the Gulf of Paria pull-apart basin (Eastern Venezuela-Trinidad). *Sedimentary Basins of the World*, **4**, 477-494 (1999).